Enabling Concurrency for Non-orthogonal LoRa Channels

Fu Yu, Xiaolong Zheng*, Liang Liu, Huadong Ma
Beijing University of Posts and Telecommunications
{yufu,zhengxiaolong,liangliu,mhd}@bupt.edu.cn

ABSTRACT

Existing LoRa only supports the concurrency of orthogonal channels but ignores the large number of non-orthogonal channel concurrency opportunities. In this paper, we propose Mc-LoRa that enables LoRa concurrency for non-orthogonal overlapping channels by solving cross-channel collision that happens when chirps with different bandwidths have the same slope in time-frequency domain. Existing single-channel concurrency methods fail to resolve this new collision because the deterministic symbol offset is invalid anymore due to the asymmetric symbol duration. But we find that when wiping a part of collided signals, the amplitude change of target chirp that aligns with the decoding window is predictable, while the collided chirps experience different changes. We accordingly regard the amplitude change ratio before and after wiping as a new decoding feature. We propose a wiper selection method based on our theoretical model to obtain robust features. We also design noise-aware wiper searching and grouping mechanisms to balance the feature accuracy and computing overhead. The experiments show that Mc-LoRa efficiently decodes packets in non-orthogonal overlapping channels and improves the network throughput by up to 3.4× under cross-channel collision, compared with the state-of-the-art single-channel concurrency methods.

CCS CONCEPTS

• **Networks → Link-layer protocols**.

KEYWORDS

LoRa, concurrent decoding, non-orthogonal channels

*Xiaolong Zheng is the corresponding author.

ACM MobiCom '23, October 2–6, 2023, Madrid, Spain

ACM ISBN 978-1-4503-9990-6/23/10…$15.00
https://doi.org/10.1145/3570361.3613268

ACM Reference Format:
Fu Yu, Xiaolong Zheng*, Liang Liu, Huadong Ma. 2023. Enabling Concurrency for Non-orthogonal LoRa Channels. In *The 29th Annual International Conference on Mobile Computing and Networking (ACM MobiCom '23), October 2–6, 2023, Madrid, Spain.* ACM, New York, NY, USA, 15 pages. https://doi.org/10.1145/3570361.3613268

1 INTRODUCTION

In the past decade, LoRa has attracted wide attention in both academy and industry [18–20, 22, 24, 33, 42, 48, 56]. Its flexible bandwidth configuration and diverse channel partition well support applications with different demand such as environmental monitoring [3, 4], video transferring [9, 41, 49, 50], contactless sensing [6, 7, 52, 53], and animal tracking [25]. Facing such ever-increasing demand of massive connectivity, LoRa's feature of large network capacity seeks to connect a large number of nodes. The limited spectrum resource is therefore becoming the bottleneck of the spectrum resource-hungry applications [11, 14, 30]. Furthermore, the increased packet collision leads to non-negligible capacity degradation, which aggravates the problem, especially when coexisting LoRa nodes whose configurations are separately controlled by different networks [28, 39, 45].

Recent studies [27, 29, 46, 54] have shown that overlapping channel partition exhibits great potential to improve spectrum efficiency and network capacity without increasing available bandwidth. As the channel plan shown in Fig. 1(a), four channels of 125 kHz and two channels of 250 kHz exist within a single channel with bandwidth (BW) of 500 kHz. Because LoRa adopts Chirp Spread Spectrum (CSS) modulation, it supports concurrent transmission with different Spreading Factor (SF) in a physical channel. Suppose each channel supports $SF$6-12, then we have 7×7 (BW, SF) pairs to establish 49 logical channels, each of which is decided by the central frequency with specific (BW, SF). Then the capacity can be significantly boosted if all of the overlapping channels can be used.

However, existing LoRa [40] only supports concurrent transmissions from orthogonal channels and seriously counteracts the benefit of using overlapping channels. This is because LoRa can only correctly decode concurrent chirps with different slopes in time-frequency domain, which requires orthogonal (BW, SF). But a group of chirps will have same slope if their (BW, SF) satisfies the rule: BW doubles and SF

increases by two, as shown in Fig. 1(b). Once $CH1$ with BW of 500 kHz is used to transmit packets, then 6 non-orthogonal channels including $CH2-7$ cannot be used simultaneously, because chirps in $CH1$ with same slope will generate multiple energy peaks in the decoding window, confusing LoRa decoding. We define this collision caused by the chirps that have the same time-frequency slopes but from non-orthogonal overlapping channels as **cross-channel collision**. Existing LoRa gateway chips such as SX1301 and SX1302 [36, 37] cannot solve cross-channel collisions and then give up utilizing non-orthogonal channels. The attractive potential of high spectrum efficiency brought by overlapping channels is fundamentally limited. This motivates us to explore enabling cross-channel concurrency for non-orthogonal LoRa channels to improve spectrum utilization.

It is non-trivial to obtain non-orthogonal concurrency because the cross-channel collision is hard to be solved by existing single-channel concurrent decoding methods. Most of the existing methods convert the time offset between collided symbols into decoding features such as peak ratio in neighboring decoding windows [44, 55], common FFT peak in successive decoding windows [8, 39], and etc. But under cross-channel collision, both the receiving time offset and the unequal symbol duration influence the features. The decoding features can be corrupted when a random symbol with asymmetric duration occurs in the decoding window.

To solve the feature failure problem, we perform in-depth analysis and find that eliminating a part of the collided signals in special frequency points has different influences on the target symbol and collided symbols. For target symbol that aligns with the decoding window, the amplitude changes after elimination are predictable while the changes of other collided symbols are random due to the asymmetric symbol duration. Accordingly, we propose a frequency wiper to perform the elimination and intentionally construct predictable features for target symbol identification. Then we can decode all the packets by regarding them as target one by one.

But enabling cross-channel concurrency by frequency wiper still has three major challenges. First, the wiper setting has to be carefully selected according to the receiving offset and symbol duration asymmetry between the target symbol and each collided symbol. Only eliminating the collided signals in special frequency points can construct the most recognizable features. But how to decide the optimal frequency wiper setting to obtain the robust features is unknown. Second, searching the optimal wiper for a single target-collided symbol pair is time-consuming, not to mention that there are multiple collided has different optimal wipers. How to balance the trade-off between feature accuracy and decoding efficiency is challenging. Third, noise can distort the decoding feature. How to decide optimal wiper under dynamic noise is challenging.

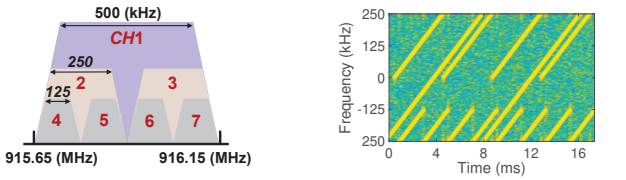

(a) Channel plan. (b) Non-orthogonal LoRa chirps.

Figure 1: (a) Channel plan with overlapping channel partitions; (b) Non-orthogonal chirps have collisions even if they have different (BW, SF)**.**

To cope with these challenges, we propose Mc-LoRa, a versatile design of LoRa gateway to enable the concurrency of non-orthogonal overlapping channels by decoding the cross-channel collisions. Firstly, Mc-LoRa adopts a wide band correlation method to efficiently detect concurrent packets in all overlapping channels by one correlation. We also identify the channel of each packet by SFD correlation peak shift analysis. Then we leverage both preamble and Start of Frame Delimiter (SFD) to eliminate Carrier Frequency Offset (CFO) and achieve accurate symbol synchronization for further decoding. Secondly, to select the optimal wiper even under dynamic noise, we carefully model the relationship between amplitude changes and the frequency wiper setting. Based on the model, we propose a wiper selection mechanism to decide the optimal wiper setting. We also design the stepwise wiper searching and wiper grouping strategies to prune wipers for a good balance between decoding accuracy and efficiency. Finally, we propose a noise-aware wiper adaption method to adjust the searching and grouping strategies for wipers of different chirps under dynamic noise.

The contribution of this paper is summarized as follow.

- To the best of our knowledge, we are the first one to reveal and resolve the new type of collision named cross-channel collision and enable the concurrency for non-orthogonal overlapping channels of LoRa.
- We design Mc-LoRa, a novel LoRa gateway solution that can concurrently decode collided packets of non-orthogonal channels. We first construct target decoding feature for decoding by frequency wiper that eliminates collided signals in specific frequency points. We also propose a noise-aware wiper selection method that decides the optimal wipers under dynamic noise, with consideration of both accuracy and overhead.
- Experimental results on both indoor and outdoor LoRa networks show that Mc-LoRa can efficiently decode concurrent transmissions from the non-orthogonal overlapping channels. Compared to state-of-the-art single-channel concurrency methods, Mc-LoRa reduces SER by up to 75.2% and improves the network throughput by up to 3.4× under cross-channel collision.

2 RELATED WORK

To receive multi-channel packets, existing commercial gateway chips such as SX1301 [36] and SX1302 [37] can utilize the SX1257 front-end sampling signal in up to 32 MHz bandwidth and divide signals into non-overlapping channels. But they cannot decode packets from non-orthogonal channels.

Many recent works focus on decoding LoRa collisions [8, 12, 39, 43, 44, 51, 55]. The key design principle is decomposing collided signals into separated chirps that can be decoded by standard LoRa. According to the process of decomposition, existing methods can be divided into two categories. Symbol matching methods recover all the chirps at once [43, 44, 55] by mapping collided chirps to corresponding packets. Symbol recognizing methods identify one target chirp at once and obtain all chirps by regarding them as targets one by one [8, 39, 51]. Both of them rely on the time offset between collided symbols to construct unique features for matching and then decoding packets.

Symbol matching methods analyze the collided chirps in successive decoding windows to cluster chirps with similar features to one packet. CoLoRa [44] and Pyramid [55] utilize the FFT peak ratio in multiple decoding windows as the feature and match chirps with similar peak ratio to one packet. NScale [43] proposes non-stationary scaling to enhance the feature. FTrack [51] uses Short Time Fourier Transform to track chirps' time offset and group them to corresponding packets. But under cross-channel collision, the asymmetric symbol duration of collided packets in different bandwidths makes the time offset based features unreliable.

Symbol recognizing methods first align the decoding window with one target symbol. Then they use the time offset between target symbol and collided symbols to divide the decoding window into multiple sub-windows and identify the target chirp according to its predictable distribution in the sub-windows. For example, CIC [39] and AlignTrack [8] leverages predictable symbol edges of interfering chirps to divide the decoding window. But under cross-channel collision, accurate symbol edge information is hard to capture because random symbols with different bandwidths cause unpredictable symbol edges.

Successive Interference Cancellation (SIC) used in Code Division Multiple Access (CDMA) is another way to achieve concurrency transmission [2, 17, 21, 32, 38]. But under cross-channel collision, SIC cannot accurately detect all the packets because it focuses on single-channel collision. What's more, it requires significant power differences of the concurrent transmissions, which is hard to satisfy in LoRa due to LoRa's inherent weak signal [16, 43, 47].

In a nutshell, existing single-channel concurrent methods cannot efficiently solve the cross-channel collision and hinder the concurrency of non-orthogonal channels.

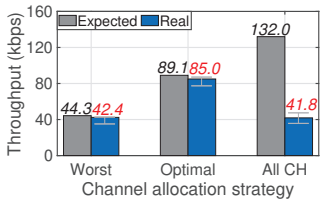

Figure 2: Throughput of 3 channel allocation strategies.

3 PRELIMINARY STUDY

3.1 Motivation

We first measure the performance gap between using orthogonal channels and using all the channels to reveal the room of improvement. We show the performance of worst and optimal channel allocation strategies when using orthogonal channels only. For a group of 7 non-orthogonal channels such as $SF12$ in $CH1$, $SF10$ in $CH2\&3$, and $SF8$ in $CH4$-7, packets with the same payload size in $CH4$-7 and $CH1$ has the shortest and longest on-air time, respectively. Hence, using $SF12$ in $CH1$ brings the lowest throughput and blocks using the other six non-orthogonal channels, resulting in the worst strategy. Conversely, using $CH4$-7 brings the highest throughput, which is the optimal strategy when using orthogonal channels only.

Since commercial gateways only support non-overlapping channels, we implement an SDR-based gateway to decode all the packets in overlapping channels. The SDR receives signals in 1 MHz bandwidth and divides I/Q samples into $CH1$-7 to perform the standard LoRa decoding (Std.LoRa) for each (BW, SF). We collect the signal traces of 49 (BW, SF) settings. In each trace, node transmits packets in maximum duty cycle. In Fig. 2, the real throughput of the worst and optimal strategy is 42.4 kbps and 85.0 kbps, respectively. The expected throughput is calculated by supposing all the packets are successfully decoded. The real throughput is close to the expected because only orthogonal channels are used. However, compared to the expected maximum throughput of using all the channels, 132.0 kbps, the channel utilization ratio of the worst and optimal strategy is only 32.1% and 64.4%. The results reveal that using only orthogonal channels significantly limits the spectrum efficiency.

However, directly using all channels suffers from serious performance degradation. The real throughput is only 41.8 kbps, much less than the expected throughput of 132.0 kbps. It motivates us to enable the concurrency for non-orthogonal channels to improve efficiency.

3.2 Problem Identification

By analyzing the packets with symbol error, we identify **cross-channel collision is the core problem that hinders the concurrency of non-orthogonal channels**. As

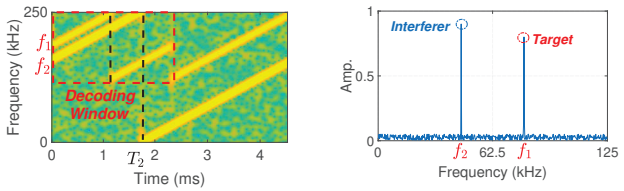

(a) Cross-channel collided chirps. (b) FFT result of one window.

Figure 3: Cross-channel collision leads to decoding errors within decoding window.

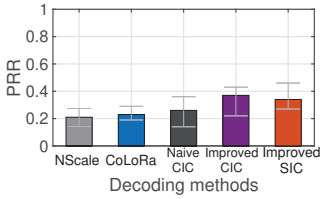

Figure 4: PRR of five single-channel concurrent decoding methods under cross-channel collision.

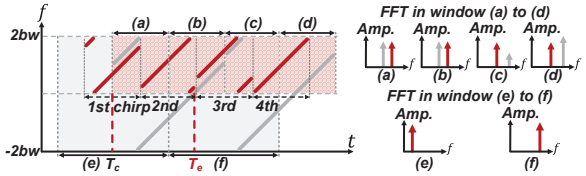

Figure 5: Illustration of feature distortions.

shown in Fig. 3(a), one non-orthogonal wider chirp exists in a symbol window of channel (bw, sf). The target chirp $C_1^{(bw,sf)}$ can be represented as

$$C_1^{(bw,sf)} = e^{j2\pi(-\frac{bw}{2}+\frac{k}{2}t)t} \times e^{j2\pi f_1 t}, t \in [0, T_{sym}^{(bw,sf)}] \quad (1)$$

where $e^{j2\pi(-\frac{bw}{2}+\frac{k}{2}t)t}$ is the basic up-chirp, $e^{j2\pi f_1 t}$ represents the frequency shift to modulate symbol, $T_{sym}^{(bw,sf)}$ is the symbol duration, $k = BW^2/2^{SF} = bw^2/2^{sf}$ is the chirp slope. A collided chirp $C_2^{(2bw,sf+2)}$ with initial frequency f_2 also appears in decoding window, which is

$$C_2^{(2bw,sf+2)} = e^{j2\pi(-\frac{bw}{2}+\frac{k}{2}t)t} \times e^{j2\pi f_2 t}, t \in [0, T_2] \quad (2)$$

Its slope $k = (2bw)^2/2^{sf+2} = bw^2/2^{sf}$ is same with $C_1^{(bw,sf)}$. To decode $r(t)$, the receiver firstly multiplies $r(t)$ with standard down-chirp $e^{j2\pi(\frac{bw}{2}-\frac{k}{2}t)t}$ and perform FFT. Then two single tone signals $e^{j2\pi f_1 t}$ and $e^{j2\pi f_2 t}$ are converted into two energy peaks in Fig. 3(b). The interference peak generated by chirp with same k leads to decoding errors when the amplitude of f_2 is higher than f_1. When multiple concurrent transmissions exist, symbol decoding will be error-prone.

3.3 Limitation of Existing Single-channel Concurrent Decoding Methods

Under single-channel collision, the error also presents as multiple confusing peaks and many methods are proposed. So a straightforward question is: can single-channel concurrency methods solve the cross-channel collision problem?

To answer this question, we apply existing single-channel concurrent decoding methods on the cross-channel collision trace, which contains 2,000 collided packets collected by SDR from experiments in Section 3.2. We implement NScale [43] and CoLoRa [44] as the representatives of symbol matching methods, CIC [39] as the representatives of symbol recognizing methods, and minimum Mean-Square Error (MMSE) based CDMA decoding with SIC which has been proven to have good performance [5, 13, 34] and widely used in recent applications [10, 15, 23]. We implement the improved version of CIC and SIC by directly providing them with receiving time information of all packets in the whole frequency band.

For each overlapping channel, we use five methods to decode collisions and measure their PRR (Packet Reception Rate). As shown in Fig. 4, the average PRR of NScale, CoLoRa, naive CIC, improved CIC, and improved SIC is 0.21, 0.23, 0.26, 0.37, and 0.34, respectively. None of them provides satisfied decoding performance.

Symbol matching methods use the predictable distribution of one symbol in multiple decoding windows as the feature to cluster symbols of the same packet. In single-channel collision, since any single chirp locates in only two successive decoding windows, the symbol offset can be converted to predictable feature such as FFT peak ratio in two successive decoding windows. But for cross-channel collision, the extracted feature from neither wide band nor narrow band is unstable due to the asymmetric symbol duration. For the example in Fig. 5, two packets with different (BW, SF) collide, described by red and gray chirps. In the narrow band decoding window, the wide chirp in gray can locate in more than two windows, depending on the modulated symbol. Its peak ratio in neighboring windows will be random. For example, the ratio of two gray peaks in window (a) and (b) is 0.5, but it is 0.33 in (c) and (d), making the FFT peak ratio invalid to cluster all the gray chirps into one packet. For the wide band decoding window, e.g. (e), the features of narrow band chirps can disappear because the short chirp can locate in only one decoding window. For example, the 1st and 3rd red chirps in Fig. 5 only locate in a single window, (e) or (f). In a nutshell, due to the asymmetric symbol duration and randomly modulated symbols, the features for decoding extracted from neither wide band nor narrow band are unreliable.

Symbol recognizing methods rely on the assumption that only the target chirp aligned with the decoding window completely spans the whole decoding window. Since there is time offset between target symbol and collided symbol, a cutting point can be found to get sub-windows where only the target peaks exist simultaneously. However, deciding accurate

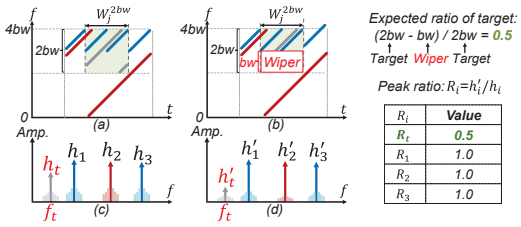

R_i	Value
R_t	0.5
R_1	1.0
R_2	1.0
R_3	1.0

Figure 6: Our observation on frequency wiping.

cutting points is difficult under cross-channel collision. On the one hand, although the out-band signals can be filtered, the chirps with narrow BW and the in-band chirp fragments from wide BW still exist and form irremovable in-band interference. Existing packet detection method can accurately detect target packets but not the interfering packets with different (BW, SF). Then the location of cutting points depending on the symbol edges of interfering packets cannot be determined. This is why the PRR of naive CIC is only 0.26. On the other hand, even if given the receiving time information of all interference packets, the cutting point is still hard to determine accurately due to unpredictable interfering chirps in wide band. In Fig. 5, the gray chirp in wide band starts in T_c, but the symbol edges T_e in window (b) cannot be inferred by T_c because it also relies on the randomly modulated symbol. Determining the cutting points by the unknown symbol edge is inaccurate. This is why the improved CIC only achieves PRR of 0.37.

SIC decodes packets in descending order of signal strength. Blindly executing SIC in each channel cannot resolve cross-channel collisions. If starting from wide band signal, the narrow band interfering packets cannot be detected. If starting from the narrow band, the signal strength of incomplete chirps can be sometimes stronger and sometimes weaker than the target, decided by the duration of chirp falling into the band. So, we improve SIC by giving it the receiving time information of packets in whole frequency. But even for improved SIC, its requirement of a clear strength difference between any two packets is hard to satisfy in practice [16, 43, 47], especially for the LoRa network deploying a large number of nodes. Any two packets with similar strengths will lead to the break of the decoding chain. Besides, LoRa allows transmission under noisy floor. But the signal with low SNR will cause inaccurate channel estimation in SIC [1, 31, 35], leading to high energy residual after subtracting and confusing the following decoding. This is why improved SIC's PRR is still low in Fig. 4.

3.4 Exploring New Decoding Features

To resolve cross-channel collision, we require a new feature to decompose collided symbols. In Fig. 6(a), three non-orthogonal chirps in (bw, sf), $(2bw, sf+2)$, and $(4bw, sf+4)$ collide with each other. Suppose the gray chirp is the target,

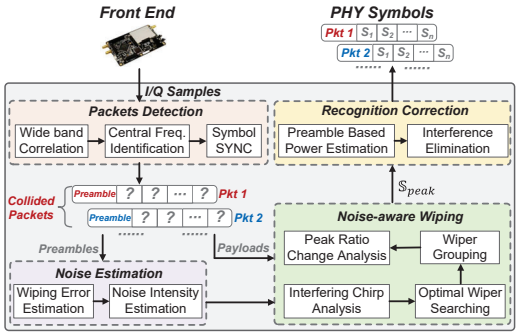

Figure 7: The overview of Mc-LoRa.

multiple peaks appear after FFT in Fig. 6(c). Theoretically, the amplitude of i-th peak can be represented by $h_i = A_i \times N_i$, where A_i is the attenuation across channel and N_i is the number of signal samples. The target symbol aligns with the decoding window and therefore N_t is known. But for other collided symbols, due to the randomness of symbols modulated in asymmetric symbol windows, N_i varies in different decoding windows and cannot be predicted. So h_i will be random and unstable. This is also why exiting concurrent decoding features fail under cross-channel collision.

We find that although the peak amplitude is unstable, its changes of the target symbol can be predictable and distinguishable when eliminating a part of the signals in special frequency points. As shown in Fig. 6(b), if we eliminate signals in the frequency band with the width of BW_{wp}, N_{wp} samples of the target chirp will be removed but the number of removed samples for other collided chirps will be different, deciding by the number of samples falling into this frequency band, which can be reflected on FFT peak amplitude changes in Fig. 6(d). Since N_t and N_{wp} are known, the amplitude change of the target symbol can be predictable while the changes of other collided symbols will be random.

Based on the above insight, we design the frequency wiper to construct a new feature for identifying the target symbol. Suppose the bandwidth of wiper in Fig. 6 is $BW_{wp} = bw$, and the initial frequency of the wiper is $f^s_{wp} = 2bw$. Chirps with different BW suffer from different frequency sample loss N_i^l, and the peak amplitude changes to $A_i \times (N_i - N_i^l)$. Then the ratio of amplitudes before and after wiping is $R_i = A_i(N_i - N_i^l)/A_iN_i$. For the target symbol, $N_t^l = N_t \frac{BW_{wp}}{2bw}$, and the change ratio $R_t = (N_t - N_t^l)/N_t = 0.5$. To identify the target peak, we can calculate the difference between R_i and the predicted R_t as $D_i = |R_i - R_t|$. Then the peak whose $D_i = 0$ is regarded as the target peak. In practice, h_i changes to $h_i + n_i$ under the impact of channel noise n_i. D_i is $\hat{D}_i = |\hat{R}_i - R_t|$ where $\hat{R}_i = (A_i(N_i - N_i^l) + n_i^2)/(A_iN_i + n_i^1)$, n_i^1 and n_i^2 are the effect of noise before and after wiping. Then for the target peak, $\hat{D}_t$ doesn't strictly equal 0. When an inappropriate wiper is used, the difference between N_i^l and N_t^l can be small,

and D_i and D_t can be indistinguishable under noise. How to select a suitable wiper to accurately identify the target symbol still need further designs.

4 DESIGN

Fig. 7 presents an overview of Mc-LoRa. After receiving signals in the widest bandwidth which covers all channels, Mc-LoRa performs packet detection to determine the number of concurrent packets and their (BW, SF), based on proposed wide band correlation method. The channel of each packet is further identified by SFD correlation peak shift analysis. Then Mc-LoRa eliminate CFO to synchronize symbol for decoding. To decode collisions, Mc-LoRa firstly estimates the channel noise for further wiper setting selection. The noise estimation executes a wiper on 8 up-chirps in the preamble to estimate the impact of noise on peak amplitude changes. The noise intensity in 8 decoding windows is also measured. Then the noise-aware wiping module selects the optimal wiper for each collided chirp. To reduce the computing overhead, we propose a noise-aware optimal wiper searching that dynamically skips the searching some starting frequency points of a wiper but has only limited influence on the decoding accuracy. Mc-LoRa also groups the wipers of different collided chirps. Then Mc-LoRa executes the final wipers one by one and calculates the amplitude change ratio for each peak. The peak that constantly satisfies the predicted change ratio in all wipers will be recognized as the target chirp. To cope with some special cases where the short chirps joined into a long chirp aligned to the target decoding window, Mc-LoRa further uses a recognition correction module to correct the results according to signal intensity.

By repeating above processes in all decoding windows, we can obtain all symbols for target packet. Then, Mc-LoRa switches to the next packet as target and performs above processes until all detected packets are decoded.

4.1 Packet Detection

Existing commercial LoRa gateway cannot detect all the packets under collision. In Fig. 8, a commercial LoRa receiver calculates the correlation between received signal and the template correlator to detect the preamble in $(2bw, sf+2)$. But the incomplete preamble in $(4bw, sf+4)$ partially overlapping with the correlator will also cause a high correlation peak. Then the receiver wrongly regards the preamble as target and processes following signal, which will miss the following true packet in channel $(2bw, sf+2)$. In short, a preamble can be processed by the multiple correlators of different channels, leading to inaccurate packet detection.

To cope with it, we propose a wide band correlation based method for detecting collided packets in overlapping channels. We utilize the insight that a wide band correlator can respond to all chirps with same slope but different (BW, SF). So, we only need one-time correlation in wide band to jointly detect all packets. Mc-LoRa defines the down-chirp $C_{down}^{(4bw,sf+4)}$ as the correlator and calculates cross-correlation with received signal to detect SFD of each packet. In Fig. 9, packets with (bw, sf) and $(2bw, sf+2)$ can both generate clear peaks. One SFD containing 2.25 down chirps generates one pair of peaks, and the interval between two peaks equals the corresponding symbol duration $T_{sym}^{(BW,SF)}$. By comparing the time interval of two peaks with three possible $T_{sym}^{(BW,SF)}$, the number of packets and corresponding (BW, SF) can be obtained.

Though above process identifies the concurrent packets, the specific channels they belong to are still unknown. In Fig. 10(a), SFDs in different channels (depicted in different colors) within the wide band correlation window will all generate correlation peaks at the beginning of the correlation window, $\hat{T}_1$. Then given the peak of SFD, the used channel is hard to determine. But the real SFD starting time of four channels with bw has a shift of 0, ΔT, $2\Delta T$, and $3\Delta T$ to $\hat{T}_1$, where $\Delta T = T_{sym}^{(bw,sf)}$. If we can measure this shift, we can determine the channel of detected SFD.

By the example in Fig. 10(b), we show how to obtain the shift x. In a wide band correlation window, we have $x + y + \Delta T = 4\Delta T$, where y is unknown. But in Fig. 10(b), the correlation peak shifts for up-chirp in the preamble equals y. And the real peak correlation locations T_2 for up-chirp and T_1 for down-chirp follow $T_1 - T_2 = 3\Delta T$ due to the LoRa packet structure. Then we can calculate x by the following equation set:

$$\begin{cases} x + y + \Delta T = 4\Delta T \\ T_1 - T_2 = 3\Delta T \\ T_2 = \hat{T}_2 + y \\ T_1 = \hat{T}_1 + x \end{cases} \tag{3}$$

where $\hat{T}_1$ and $\hat{T}_2$ can be obtained by correlation and ΔT is known. Then x, y, T_1, and T_2 can be calculated to identify the used channel. In practice, CFO caused by asynchronous clocks is inevitable. Though estimation errors of T_1 and T_2 caused by CFO do not influence channel usage identification, eliminating CFO is necessary for symbol SYNC and the following decoding. Hence, we adopt similar CFO elimination method with previous works [8, 43, 44]. Then for collided packets, we perform the following decoding processes.

4.2 Modeling Optimal Wiper

We model the relationship between wiper and the feature robustness to select the optimal wiper. Fig. 11(a) shows a collision example that contains a target chirp in $BW_t = 4bw$

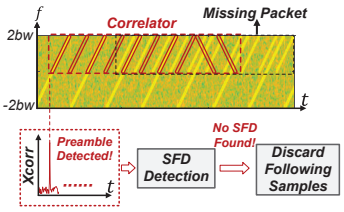

Figure 8: The packet detection errors caused by cross-channel collision.

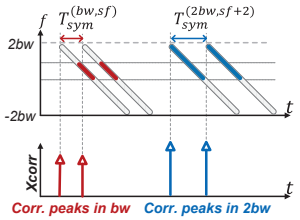

Figure 9: The correlation peaks generated by a wide band down-chirp.

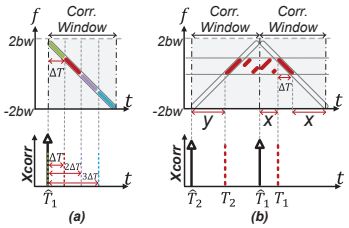

Figure 10: Identify the used channel by both preamble and SFD.

and the interfering chirps in $BW_C = 2bw$. We use the interfering chirp C3 as the illustration example. Chirp C3 falls into the decoding window with bandwidth BW_I from f_I^s and f_I^e. When performing FFT on BW_t, we will get multiple peaks, each peak corresponds to one chirp.

In Fig. 11(b), if we perform a wiper with bandwidth of $BW_{wp} = 0.5bw$, from f_{wp}^s to f_{wp}^e, then the FFT peak amplitudes change because the wiper eliminates a part of signal samples and leads to signal energy loss. The expected amplitude change of the target chirp is $(BW_t - BW_{wp})/BW_t = (4bw - 0.5bw)/4bw$, which is 0.875. The channel noise also influences the peak amplitude changes, the amplitude change ratio $\hat{R}_i$ of C1, C2, C3, and target are 0.50, 0.74, 0.87, and 0.80. Then C3 will be wrongly regarded as the target because its change ratio is closest to the predicted value. Besides, one wiper has different influence on different collided chirps under noise, depending on the BW_I of the collided chirps. The optimal wiper can be different for different collided chirps. Hence, the wiper should be carefully designed.

To select the optimal wiper, we carefully model the relationship between wiper and caused energy loss. Without losing generality, we illustrate the model considering the target symbol and one interference chirp for simplicity. Denote R_I as the amplitude change ratio of an interference chirp after wiping and D_I as the difference between R_I and the expected change ratio of the target R_t. Based on the analysis in Section 3.4, we know that $R_i = (N_i - N_i^l)/N_i$ for the i-th peak, where N_i and N_i^l is the number of signal samples before and after wiping. According to the relative position of wiper and interfering chirp, R_I can be calculated as:

$$R_I = \begin{cases} 1, \ f_{wp}^s \in [0, f_{wp}^e], f_{wp}^e \in [0, f_I^s] \\ 1 - \frac{f_{wp}^e - f_I^s}{BW_I}, \ f_{wp}^s \in [0, f_I^s), f_{wp}^e \in [f_I^s, f_I^e) \\ 1 - \frac{f_{wp}^e - f_{wp}^s}{BW_C}, \ f_{wp}^s \in [f_I^s, f_{wp}^e), f_{wp}^e \in [f_I^s, f_I^e) \\ 1 - \frac{f_I^e - f_{wp}^s}{BW_C} \ f_{wp}^s \in [f_I^s, f_I^e), f_{wp}^e \in [f_I^e, BW_t] \\ 1, \ f_{wp}^e \in [f_I^e, f_{wp}^e], f_{wp}^e \in [f_I^e, BW_t] \end{cases} \quad (4)$$

Though Eq. (4) is a little bit complex due to the various relative positions between the wiper and interfere chirp, it is not hard to derive because all the cases follow the same calculation principle, i.e., the ratio of remaining signal energy to the original signal energy. Hence, we omit the formula derivation details and only present the result. Then D_I can be calculated $D_I = |R_I - R_t|$. Since we cannot control the random channel noise, we can only select a wiper setting that enlarges D_I as much as possible to avoid errors.

The maximum $D_I = (BW_t - BW_I)/BW_t$ is obtained when the wiper selects the setting, $BW_{wp} = BW_I$ and $f_{wp}^s = f_I^s$. The selected wiper is shown in Fig. 12(a). We can find that the optimal wiper completely overlaps with the interfering chirp and the peak amplitude of the interfering chirp after wiping is around 0. Meanwhile, there is another equivalent wiper setting that can also make D_I equal to the same maximum, which is $f_{wp}^s = f_I^e$ and $BW_{wp} = BW_t - BW_I$, as shown in Fig. 12(b). In this case, the wiper and interfering chirp do not overlap at all. Then the peak amplitude of the interfering chirp after wiping is basically unchanged, but the amplitude of the target peak significantly decreases because most of the effective signal samples are eliminated. But under the influence of channel noise, too small amplitude can cause the target peak undetectable. Hence, Mc-LoRa uses the optimal wiper with smaller BW_{wp}:

$$BW_{wp} = min\{BW_I, BW_t - BW_I\} \quad (5)$$

Then the starting frequency of the wiper, f_{wp}^s is:

$$f_{wp}^s = \begin{cases} f_I^s, \ BW_{wp} = BW_I \\ f_I^e, \ BW_{wp} = BW_t - BW_I \end{cases} \quad (6)$$

Though the feature is proposed for cross-channel collision, it also works for single-channel collision where collided packets use the same channel. In single-channel collision, the existence of symbol time offset makes one target decoding window includes two neighboring interfering chirps from one concurrent packet. Then the two interfering chirps that modulate different symbols will generate two energy peaks in different FFT bins. Since the wiper partially overlaps with the two chirps, the energy loss caused by wiper will be distributed to two peaks with a ratio determined by the relative position between interfering chirps and wiper. Due to the randomness of modulated chirps, D_I will not always be close to D_t when performing multiple wipers. Hence, Mc-LoRa can also resolve the single-channel collision.

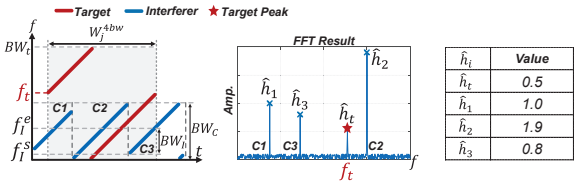

$\hat{h}_i$	Value
$\hat{h}_t$	0.5
$\hat{h}_1$	1.0
$\hat{h}_2$	1.9
$\hat{h}_3$	0.8

(a) FFT result under cross-channel collision.

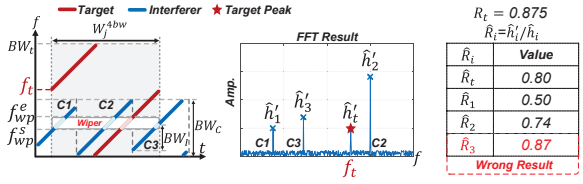

$\hat{R}_i$	Value
$\hat{R}_t$	0.80
$\hat{R}_1$	0.50
$\hat{R}_2$	0.74
$\hat{R}_3$	0.87

Wrong Result

(b) Peak amplitude changes after wiping.

Figure 11: The unsuitable wiper destroys the feature.

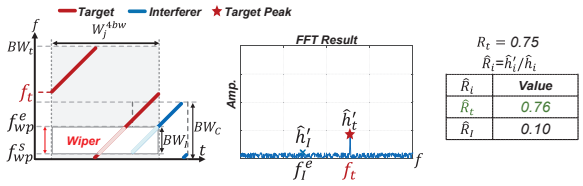

$\hat{R}_i$	Value
$\hat{R}_t$	0.76
$\hat{R}_I$	0.10

(a) Optimal wiper setting 1.

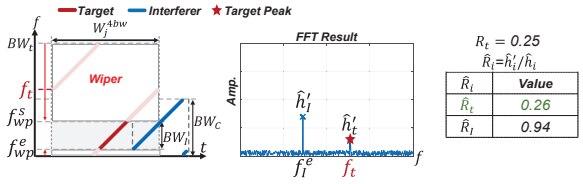

$\hat{R}_i$	Value
$\hat{R}_t$	0.26
$\hat{R}_I$	0.94

(b) Optimal wiper setting 2.

Figure 12: Two optimal wiper settings.

4.3 Noise-aware Wiper Selection

4.3.1 Interfering Chirp Analysis. In practice, multiple collided chirps can exist in one decoding window. Suppose that the target packet collides with M packets and the data payload of m-th packet Pkt_m and target packet Pkt_t start at T_m and T_t. We firstly estimate N_c^m, the number of collided chirps of Pkt_m in the decoding window. Given the bandwidth, payload starting time, and symbol duration of Pkt_t and Pkt_m. Since the bandwidths of overlapping channels are in integral multiples, if the payload starting time of Pkt_t and Pkt_m aligns, then the following symbols are also aligned with multiples. When $BW_t > BW_m$, $N_c^m = BW_t/BW_m$. Otherwise, N_c^m is 1. If the payload starting time of Pkt_t and Pkt_m has an offset, the following symbols will partially overlap with each other. When $BW_t > BW_m$, N_c^m equals $BW_t/BW_m + 1$. When $BW_t \leq BW_m$, the interfering chirp has a long duration and only one or two chirps fall into the narrow band decoding window, depending on whether the interfering symbol crosses the decoding window boundary.

4.3.2 Optimal Wiper Searching. According to Eq. (5) and (6), we need to learn BW_I to determine the wiper with BW_{wp} and f_{wp}^s for each collided chirp. As illustrated in Fig. 13, when the bandwidth of the interfering chirp is larger than BW_t, i.e. $BW_m > BW_t$, its BW_I and f_I^s depend on the modulated symbol, which is unknown. If N_c^m is 1 (e.g., $W_{j+1}^{BW_t}$ in Fig. 13), BW_I is in $[0, BW_t]$. If N_c^m is 2 (e.g., $W_j^{BW_t}$ in Fig. 13), the BW_I is in $[0, BW_I^{valid}]$, where BW_I^{valid} for the first and second part of the chirp is $BW_t \cdot \Delta T_I / T_{sym}^{(BW_t, SF_t)}$ and $BW_t \cdot (1 - \Delta T_I / T_{sym}^{(BW_t, SF_t)})$, respectively. Then the most naive yet accurate selection method is searching all the possible values of BW_I and f_I^s by executing the wiper.

When the interfering chirp is in narrow band, i.e. $BW_m \leq BW_t$, as shown in Fig. 14, BW_I can be directly calculated according to the time duration of the chirp in the decoding window. For example, in Fig. 14, BW_I of the first and last interfering chirp is $BW_m \cdot (1 - \Delta T_I T_{sym}^{(BW_m, SF_m)})$ and $BW_m \cdot \Delta T_I T_{sym}^{(BW_m, SF_m)}$, respectively. Though BW_I can be calculated, we still need searching f_I^s in $[0, BW_m]$, which brings large computing overhead. To cope with it, we propose stepwise wiper searching mechanism that searches the optimal BW_{wp} and f_{wp}^s with a step of f_{step}. With a proper f_{step}, Mc-LoRa balances wiper selection accuracy and computing overhead.

4.3.3 Wiper Grouping. After above process, we can obtain an optimal wiper for a specific collided chirp. But the selected wipers for multiple collided chirps can have similar settings. So we propose a wiper grouping mechanism to reduce the redundancy. Specifically, we gather multiple wipers to one group when the difference of their BW_{wp} and f_{wp}^s are smaller than f_g. In each group, we use the average value of all BW_{wp} and f_{wp}^s to synthesize a representative wiper. Then we execute this synthesized wiper instead of all wipers in the group to reduce computing overhead.

4.3.4 Noise-aware Wiper Adaptation. Though the step-wise searching and wiper grouping reduce computing overhead, they bring estimation errors between the used wiper and the optimal wiper. With a step size of f_{step}, the step-wise searching brings an error within $f_{step}/2$ for BW_{wp} and f_{wp}^s. The maximum estimation error brought by wiper grouping is f_g for BW_{wp} and f_{wp}^s.

Using the wiper settings with maximum deviation of $\delta_f = f_g + f_{step}/2$ can distort the feature. As illustrated in Fig. 12(a), the optimal wiper is expected to eliminate the whole interfering chirp, then $BW_{wp} + \delta_f$ has no influence on interfering chirp but eliminates more of the target chirp. Then it incurs a decrease of δ_f / BW_t to R_t because $R_t = (BW_t - (BW_{wp} + \delta_f))/BW_t$. Given the wiper bandwidth unchanged, the searching error of f_{wp}^s will lead to an interfering chirp having a remaining part with bandwidth of δ_f missing the

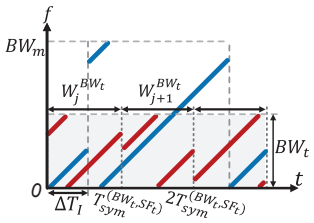

Figure 13: Wide band interfering chirps.

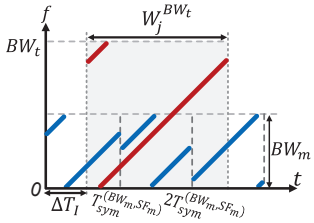

Figure 14: Narrow band interfering chirps.

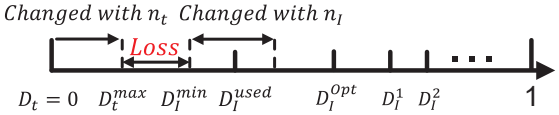

Figure 15: The tolerance of feature distortions.

wiping. It incurs an increase of δ_f/BW_t to R_I because $R_I = (BW_I - (BW_{wp} - \delta_f))/BW_I$. Then the maximum error of D_I caused by searching and grouping is $\delta_f/BW_t + \delta_f/BW_I$. For simplicity, we define $Loss = \delta_f/BW_t + \delta_f/BW_I$. Namely, $D_I^{used} = D_I^{Opt} - Loss$. Suppose the noise influence the wiping result by n_I, the minimum D_I^{min} is $D_I^{used} - n_I$. D_t is calculated but not searched, and therefore only has a wiping error n_t caused by noise, then the maximum D_t^{max} is $D_t + n_t$.

If f_{step} and f_g are too large, then D_I^{min} can be smaller than D_t^{max}, leading to feature errors and consequent peak recognition failures, as shown in Fig. 15. Hence, we need carefully select f_{step} and f_g to reduce the computing overhead maximally while keeping D_I^{min} larger than D_t^{max}, i.e.,

$$Loss < D_I^{Opt} - D_t - n_I - n_t \tag{7}$$

where D_t is known. D_I^{Opt} can be obtained when wiping the interfering chirp with the maximum BW_I among all chirps because $D_I = |BW_{wp}/BW_t - BW_{wp}/BW_I|$. If the chirp with the maximum BW_I is in narrower band than the target, D_I^{Opt} can be directly calculated because BW_I can be calculated based on the analysis in Section 4.3.2. If the chirp with the maximum BW_I is in wider band than the target, BW_I is unknown. Hence, we estimate it as the expected value, $BW_I^{valid}/2$, where BW_I^{valid} is defined in Section 4.3.2.

Under dynamic noise, Mc-LoRa learns n_I and n_t by the noise estimation module and calculates the right part of Eq. (7). Then Mc-LoRa adjusts f_{step} and f_g to get a suitable $Loss$ to satisfy Eq. (7). For simplicity, in our current implementation, we let $f_{step} = f_g$. Then they can be calculated directly, because $\delta_f = f_g + f_{step}/2$. After deciding the most suitable wipers for all collided chirps under current noise, Mc-LoRa iteratively executes the wipers and regards the peak whose $\hat{D}_i$ constantly below D_t^{max} as the target peak, the selected peak is output to the set of candidate targets, $\mathbb{S}_{peak}$.

We measure the computing overhead by the number of FFT operations, which is the most time-consuming operation

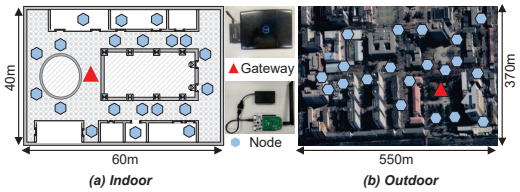

Figure 16: The indoor and outdoor LoRa network.

in the whole decoding. Mc-LoRa aligns the decoding window with each symbol for decoding. Suppose K packets collide, the payload of each has L symbols. Then the total number of symbols to decode can be represented by $K \times L$. In each decoding window, the number of optimal wipers equals to the number of interfering chirps, which is decided by K. Each wiper performs FFT once. The computing complexity is $O(K^2)$ with the increase of collided packets.

4.4 Recognition Correction

In practice, $\mathbb{S}_{peak}$ can contain more than one peak in the following three corner cases. (1) The interfering chirps span the whole decoding window like the target chirp. Suppose the wide band chirp with 500 kHz bandwidth modulates random symbols, the probability that it spans the whole decoding windows in 125 kHz is $1/2^{SF}$. It will be highest when $SF = 6$, which is 1.56%. (2) The single-channel collided packet has the same consecutive symbols. When transmitting random symbols, the probability of this case is $(1/2^{SF})^2$, it will be highest when $SF = 6$, which is 0.02%. (3) Interfering chirps with BW_t and has a very small symbol offset with target chirp. The occurrence probability depends on the channel access time offsets of concurrent packets.

To avoid decoding errors, we use the recognition correction module to remove the false targets. We rely on the insight that all chirps in one packet suffer similar attenuation, which results in similar FFT peak amplitude. So, we leverage the peak amplitudes in the preamble to learn the peak amplitude of target symbols. Then we check the amplitude of all candidate target peaks in $\mathbb{S}_{peak}$ and remove the collided peaks with different amplitudes.

5 EVALUATION

5.1 Implementation & Experimental Setup

We implement a prototype of Mc-LoRa consisting of front end and software decoding. The front end is implemented by Hack-RF with receiving bandwidth of 1 MHz to cover the widest channel. Then, we implement the decoding module by Matlab on laptop. After obtaining I/Q samples, Mc-LoRa divides the collided chirps according to the slope in time-frequency domain and decodes collisions with different slopes in parallel.

We evaluate Mc-LoRa in both indoor and outdoor LoRa networks. In Fig. 16(a), the indoor network consists of 20

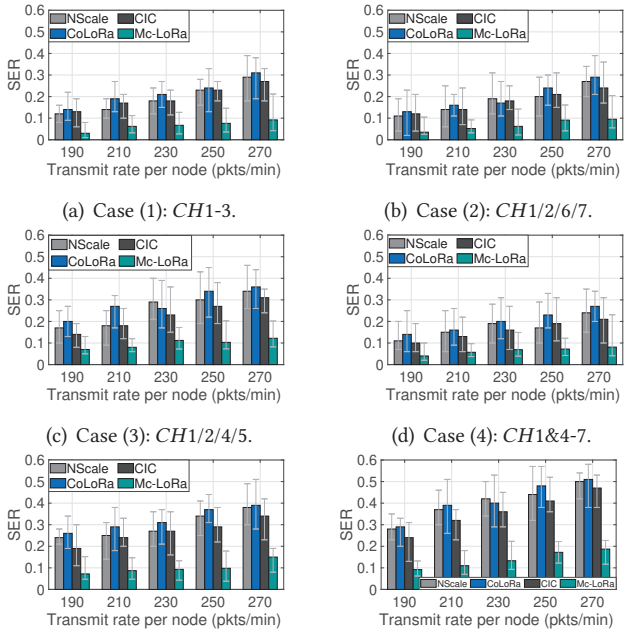

(a) Case (1): $CH$1-3. (b) Case (2): $CH$1/2/6/7.

(c) Case (3): $CH$1/2/4/5. (d) Case (4): $CH$1&4-7.

(e) Case (5): $CH$1/2&4-7. (f) Case (6): $CH$1-7.

Figure 17: The average SER under cross-channel collision with 6 channel usage cases.

nodes (depicted as hexagons) with SX1262 radio chip and STML073RZ MCU, in 2,400 m^2 office. We also deploy 20 nodes in 203,500 m^2 campus to evaluate Mc-LoRa in outdoor environment, as shown in Fig. 16(b). The SNR of indoor and outdoor network varies in [-5,20] dB and [-20,20] dB. Similar to existing studies [26, 43], we collect raw received signals of nodes in all 49 channels shown in Fig. 1(a). In each trace, the node transmits packets with a 20-byte payload in the maximum duty cycle, using default CR (Coding Rate) of 4/5. The traffic pattern in each trace follows a uniform distribution. We combine traces to emulate collisions. We randomly select the traces to emulate collisions under different conditions such as different numbers of concurrent nodes.

For comparison, we implement six single-channel concurrent decoding methods, including NScale, CoLoRa, CIC and improved CIC, SIC and improved SIC. The collided signals will be divided into 7 separate channels and decoded by the above six methods.

5.2 Performance under Different Collisions

5.2.1 Cross-channel Collisions. We first compare Mc-LoRa and baselines under cross-channel collision. We select data traces with three groups of non-orthogonal (BW, SF) settings, $SF$6-8-10, $SF$7-9-11, and $SF$8-10-12 for BW=125 kHz, 250 kHz, 500 kHz to obtain 6 cross-channel collision cases. The channels used in 6 cases change from simple to complex: (1) $CH$1-3, (2) $CH$1/2/6/7, (3) $CH$1/2/4/5, (4) $CH$1&4-7, (5) $CH$1/2&4-7, and (6) all 7 channels: $CH$1-7. The channel ID

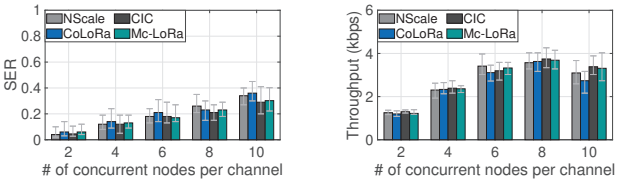

(a) SER. (b) Throughput.

Figure 18: Performance under single-channel collision in $CH$1 and $SF$11.

is consistent with the channel partition in Fig. 1(a). In each case, each channel has only one node transmitting to get only cross-channel collision traces. We use nodes in different locations to generate collided signals with different SNR.

In Fig. 17(a)-(f), we can clearly find that the SER of Mc-LoRa is the lowest among 4 methods in all 6 cases. With the increase of transmit rate, the SERs of all the methods increase because the collision possibility increases. The average SER in case (4) is lowest among 6 cases even though more channels are used than case (1)-(3). This is because $CH$4-7 with 125 kHz bandwidth only collide with $CH$1 separately but are orthogonal with each other. Though having the minimum collision intensity in case (4), when the transmit rate is 270 pkts/min, Mc-LoRa still reduces the average SER by 66.0%, 70.6%, and 61.9%, compared with NScale, CoLoRa, and CIC. In case (6) Where $CH$1-7 are used, the cross-channel collision intensity is highest and the SERs of four methods all increase. When the transmit rate per node is 270 pkts/min, the SERs of three baselines are 0.50, 0.51, and 0.47, respectively. Such high SER cannot support reliable transmission. However, Mc-LoRa can keep average SER to 0.19, which is 62.0%, 62.7%, and 59.5% lower than the SER of NScale, CoLoRa, and CIC. The results demonstrate that Mc-LoRa can efficiently resolve the cross-channel collision which is hard to solve using single-channel concurrent decoding methods.

5.2.2 Single-channel Collision. We synchronize multiple data traces with 500 kHz & $SF$11 in $CH$1 to emulate single-channel collisions. The transmit rate per node is 270 pkts/min. In Fig. 18(a), when the number of concurrent nodes increases from 2 to 10, the SERs of all methods increase as expected. Overall, Mc-LoRa achieves similar performance with the other three single-channel concurrency methods. When the number of concurrent nodes is beyond 8, all four methods have performance degradation. When there are 10 concurrent nodes, the average SER of Mc-LoRa, NScale, CoLoRa, and CIC is 0.34, 0.36, 0.29, and 0.30. The throughput of 4 methods is 3.09, 2.73, 3.38, and 3.31 kbps in Fig. 18(b).

5.2.3 Hybrid Collision. In practice, cross- and single-channel collisions can happen at the same time. Hence, we evaluate Mc-LoRa under hybrid collision. We select channel usage case (6) and vary the number of nodes in each channel. The

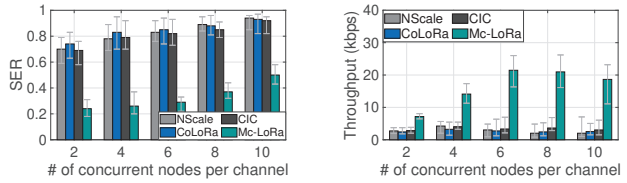

(a) SER. (b) Throughput.

Figure 19: Performance under hybrid collision in channel usage case (6).

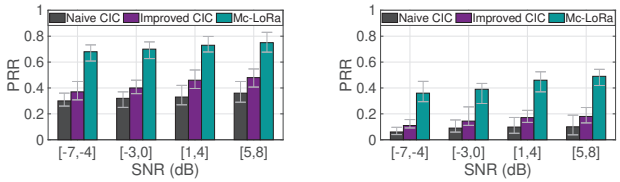

(a) Cross-channel collision. (b) Hybrid collision.

Figure 20: Performance under collisions with different SNR in channel usage case (6).

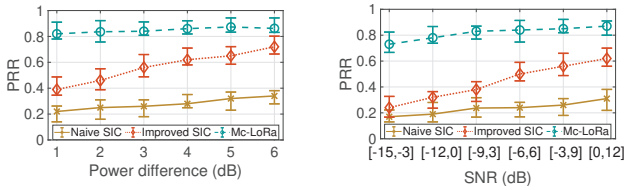

(a) Various power difference. (b) Various SNR.

Figure 21: Performance of SIC under different power difference and SNR in channel usage case (3).

transmit rate per node is 270 pkts/min. In Fig. 19(a), when the number of concurrent nodes per channel increases from 2 to 10, the SER of NScale, CoLoRa, and CIC increases from 0.70, 0.74, and 0.69 to 0.94, 0.93, and 0.92, while the SER of Mc-LoRa increases from 0.24 to 0.50. The maximum throughput of Mc-LoRa can be up to 21.4 kbps when 6 concurrent nodes transmit in each channel, which is 4.1×, 5.6×, and 4.3× higher than NScale, CoLoRa, and CIC. When there are 10 concurrent nodes, the throughput of Mc-LoRa drops to 18.6 kbps which is still 8.0×, 6.2×, and 5.1× higher than the throughput of the other three methods.

5.3 Comparison with CIC and SIC

We give packet receiving time information to CIC and SIC to verify whether cross-channel collision can be resolved.

5.3.1 Comparison with Improved CIC. We compare Mc-LoRa with CIC and improved CIC under two types of collision. The transmit rate per node is 270 pkts/min. In Fig. 20(a), the PRR of three methods improves when SNR increases, and the average PRR of the three methods is 0.33, 0.43, and 0.72 respectively. Fig. 20(b) shows the PRR under hybrid collision with 10 nodes per channel, Mc-LoRa achieves an average PRR of 0.43, which is 3.7× and 1.9× higher than naive CIC and improved CIC. The results demonstrate that even if providing accurate packet information, CIC cannot decode cross-channel collisions well because the randomly modulated symbols have unpredictable collided chirp edges, resulting in corrupted decoding features.

5.3.2 Comparison with SIC. We compare Mc-LoRa with SIC and improved SIC under different power differences. Suppose that the SNR of four collided packets are arranged in ascending order, the power difference is defined as the absolute value of SNR difference of any two packets whose SNR are most closed. In Fig. 21(a), we maintain the average SNR of collided packets to 3 dB to avoid the influence of noise. When the power difference is 1 dB, the PRR of SIC and improved SIC are only 0.22 and 0.39 while Mc-LoRa still maintains PRR to 0.82. When the power difference increases to 6 dB, the PRR of SIC only increases to 0.34. Directly using SIC for separate collided packets is invalid due to the lack of packet information. Even for improved SIC which has receiving time information, distinct power differences are necessary for good performance. But it's hard to satisfy in LoRa networks with a large number of nodes.

What's worse, SIC is also affected by the SNR of collided packets, authors in [1, 31, 35] show that low SNR reduces the accuracy of channel estimations and leads to high energy residue after subtracting the recovered signal from the collided signal. In Fig. 21(b), we maintain power difference to 3 dB to satisfy the requirement of clear signal strength difference. When SNR decreases from [0,12] dB to [-15,-3] dB, the PRR of improved SIC significantly decreases from 0.62 to 0.24 while Mc-LoRa can always keep the PRR higher than 0.70. It reveals that SIC cannot resolve collisions in lower SNR (e.g. SNR<0). But transmission under lower SNR is one of LoRa's key features. Meanwhile, low SNR also makes the FFT peak unstable which makes naive SIC have low PRR.

5.4 Performance under Different Scenarios

5.4.1 Different SF and Coding Rate. We verify Mc-LoRa regarding *SF* in Fig. 22(a). When using smaller *SF*, *SF*6-8-10, the SER increases significantly from 0.12 to 0.28 when SNR decreases from [5,8] to [-7,-4] dB. It indicates that channel noise indeed influences the frequency wiping results. Using the larger *SF* of *SF*8-10-12 has less SER degradation. Under the low SNR in [-7,-4] dB, the average SER for *SF*6-8-10, *SF*7-9-11, and *SF*8-10-12 is 0.28, 0.23, and 0.18.

In Fig. 22(b), we verify Mc-LoRa regarding *CR* under hybrid collision. Using *CR* 4/8 can significantly improve the PRR under collision because lower *CR* brings stronger error correction ability. It can keep PRR higher than 0.85 when the number of concurrent nodes is less than 6. When more than 6 nodes transmit in each channel, heavy collisions cause more

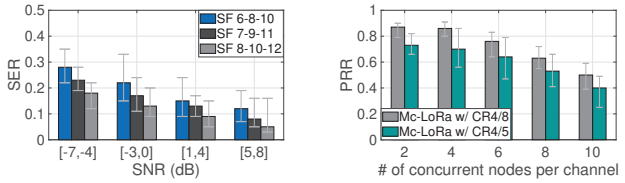

(a) *SF*. (b) *CR*.

Figure 22: Performance under different transmission configurations in channel usage case (6).

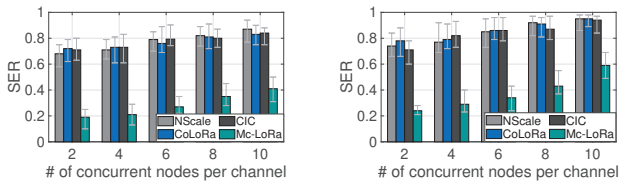

(a) LOS. (b) NLOS.

Figure 23: Performance under LOS and NLOS scenarios in channel usage case (6).

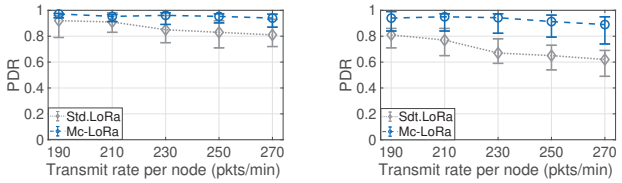

(a) Case (4): *CH*1&4-7. (b) Case (6): *CH*1-7.

Figure 24: The packet detection rate in channel usage case (4) and (6).

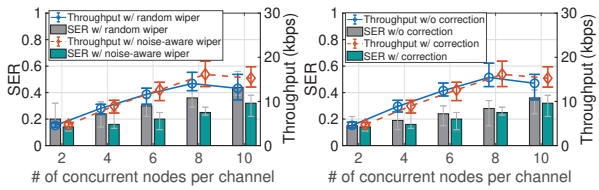

(a) Wiper setting selection. (b) Recognition correction.

Figure 25: Ablation experiments under hybrid collision in channel usage case (3).

errors which are beyond the ability of correction. Compared with *CR* 4/5, using *CR* 4/8 can improve PRR by 14.2% on average. To further improve PRR, more forward error correction methods such as concatenated code can be used.

5.4.2 LOS and NLOS Scenarios. We further investigate the performance of Mc-LoRa in LOS and NLOS scenarios under hybrid collisions with the same setting of Fig. 19(a). In Fig. 23, compared to LOS scenario, the SER of all 4 methods in NLOS increases. But Mc-LoRa still achieves the lowest SER. When using 10 concurrent nodes, the average SER of Mc-LoRa in LOS and NLOS is 0.41 and 0.59. For NScale, CoLoRa, and CIC, the SER in NLOS is 0.95, 0.95, and 0.94, which is 9.1%, 14.4%, and 11.9% higher than the SER in LOS.

5.5 Evaluation of Mc-LoRa's Main Modules

5.5.1 Packet Detection Accuracy. Accurate packet detection is the prerequisite for decoding. Hence, we measure the Packet Detection Rate (PDR) of Mc-LoRa and Std.LoRa under using channel cases (4) and (6). We only treat the detected results with accurate packet information as the detected packets. Only when (1) the detection error of start time is less than one sampling interval (i.e. 2 ms for bandwidth of 500 kHz) and (2) the correct bandwidth and central frequency are identified, the packet is regarded as detected. As shown in Fig. 24, for both cases, the increase of transmit rate causes more collisions and the PDR decreases correspondingly. When using all 7 channels in case (6), the PDR of Std.LoRa significantly drops with the increased transmit rate. But Mc-LoRa can keep PDR above 0.85 even when the transmit rate is 270 pkts/min, while Std.LoRa can only achieve PDR of 0.62.

5.5.2 Noise-aware Wiper Setting Selection. We use the wiper model and estimated noise to efficiently search the optimal wiper and further group wipers to reduce computing overhead. We verify the efficiency of wiper setting selection by ablation experiments. The transmit rate per node is 270 pkts/min. In Fig. 25(a), the SER of Mc-LoRa is obviously lower than using random wiper setting. Overall, the SER can be reduced by 24.2% on average when using the wiper selection module. The throughput is improved by 17.8% when 10 nodes transmit in each channel. We also study the efficiency of the recognition correction module. In Fig. 25(b), the recognition correction can reduce SER by 10.7% on average. And the throughput is improved by 7.6% when there are 10 nodes transmitting in each channel.

Then we evaluate the noise-aware wiper adaptation mechanism under cross-channel collision. Note that Mc-LoRa adjusts the loss setting based on noise to balance the decoding accuracy and computing overhead. The higher the loss setting is, the larger step size is used for wiper searching and the more wipers are pruned during grouping, resulting in less computing overhead. But a high loss will make the difference between target symbol and collided symbol smaller, leading to more decoding errors. We verify whether Mc-LoRa can select the suitable loss setting under cross-channel collision in channel usage case (3). We keep the SNR around 5 dB and vary the loss from 0.1 to 0.7. The computing overhead is measured by the number of wipers used for decoding target chirp in a decoding window. From Fig. 26, we can find that the increase in loss leads to increased SER and reduced wipers per symbol. A loss setting of 0.5 achieves a good trade-off because the SER significantly increases and the decrease of

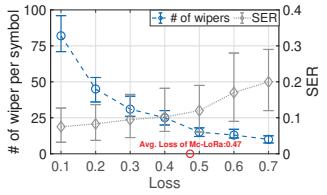

Figure 26: Decoding accuracy and computing overhead under different loss settings.

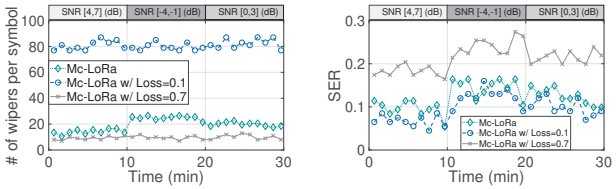

(a) Computing overhead. (b) SER.

Figure 27: Performance under cross-channel collision with dynamic noise in channel usage case (3).

computing overhead slows down after 0.5. We also record the average loss chosen by Mc-LoRa, which is 0.47.

We further demonstrate the performance of Mc-LoRa under dynamic noise. In Fig. 27, Mc-LoRa with low fixed loss of 0.1 can always achieve smaller SER but have much more wipers to execute. On the contrary, Mc-LoRa with high fixed loss of 0.7 has the lowest computing overhead but much higher SER. Mc-LoRa can efficiently adjust the used number of wipers to reduce the computing overhead but avoid serious SER increase. Compared with using the fixed loss of 0.1, Mc-LoRa significantly reduces the computing overhead by 79.0% on average and maintains a similar SER.

5.6 Performance in Large-scale Network

To evaluate Mc-LoRa in large-scale networks, we emulate the transmissions of different numbers of concurrent nodes using the traces collected in all 49 overlapping channels. We evaluate the throughput under 5 different strategies that belong to two categories: (1) using all 49 channels and Mc-LoRa, Std.LoRa and CIC to decode (denoted as Mc-LoRa-49, Std.LoRa-49, and CIC-49); (2) using only orthogonal channels and CIC to decode, 19 and 34 channels are used in the worst and optimal strategies (denoted as CIC-19 and CIC-34).

In Fig. 28. the network throughput of Mc-LoRa-49 keeps increasing until the number of concurrent nodes reaches 330. But for Std.LoRa-49 and CIC-49, the throughput decreases when the number of concurrent nodes is larger than 90 and 210, respectively. The corresponding highest throughput is 23.8 kbps and 56.3 kbps for Std.LoRa-49 and CIC-49, which are 82.1% and 57.7% lower than Mc-LoRa-49. When only using orthogonal channels, CIC-34 and CIC-19, their throughput can be good when the number of concurrent nodes is small due to single-channel collision decoding ability. But

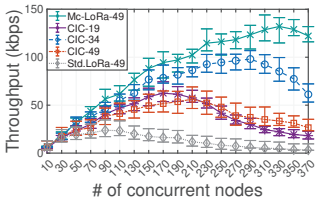

Figure 28: Performance in large-scale indoor network.

when the number of concurrent transmission exceeds the collision decoding ability, CIC's performance drops sharply. The maximum throughput of CIC-34 and CIC-19 only is 98.1 kbps and 62.5 kbps, which is 30.6% and 52% lower than the maximum throughput of Mc-LoRa-49 because fewer channels they use. CIC-19 has a much lower throughput because it uses wide channels that hinder using high-capacity narrow channels. Thanks to the full utilization of channels, Mc-LoRa further supports 330 nodes before throughput decreases. When the number of concurrent nodes is 370, Mc-LoRa still achieves the throughput of 118.2 kbps, which is 3.4× higher than CIC-34. The results clearly demonstrate that Mc-LoRa can enable the non-orthogonal channel concurrency and significantly improve the spectrum efficiency.

6 CONCLUSION

In this paper, we propose Mc-LoRa that enables the concurrency of non-orthogonal overlapping channels and significantly improves the spectrum efficiency. We identify the key obstacle as a new type of LoRa collision named cross-channel collision, which is generated by chirps with different bandwidths but the same slope in time-frequency domain. The decoding features used by existing methods are corrupted by cross-channel collision. we explore a new insight that wiping a part of collided signal cause the predictable amplitude changing of target chirp in aligned decoding window. We establish the model between wiper setting and the energy loss to select the optimal wiper setting. To balance the trade-off between accuracy and computing overhead, we further propose the noise-aware wiper searching and wiper grouping mechanisms. The extensive experimental results demonstrate that Mc-LoRa can improve network throughput by up to 3.4× under cross-channel collision, compared to existing single-channel concurrency methods.

ACKNOWLEDGMENTS

This work is supported in part by the National Key Research and Development Program of China (No. 2021YFB2900100), the Funds for Creative Research Groups of China (No. 61921003), the National Natural Science Foundation of China (No. 62072050 and No. 62225204), the A3 Foresight Program of NSFC (No. 62061146002), Xiaomi Young Talents Program of Xiaomi Foundation, and BUPT Excellent Ph.D. Students Foundation (No. CX2022124).

REFERENCES

[1] Jeffrey G Andrews and Teresa H Meng. 2003. Optimum power control for successive interference cancellation with imperfect channel estimation. *IEEE Transactions on Wireless Communications* 2, 2 (2003), 375–383.

[2] Jeffrey G Andrews and Teresa H-Y Meng. 2004. Performance of multicarrier CDMA with successive interference cancellation in a multipath fading channel. *IEEE Transactions on Communications* 52, 5 (2004), 811–822.

[3] Yosi Apriani, Wiwin A Oktaviani, and Ian Mochamad Sofian. 2022. Design and Implementation of LoRa-Based Forest Fire Monitoring System. *Journal of Robotics and Control* 3, 3 (2022), 236–243.

[4] Pietro Boccadoro, Biagio Montaruli, and Luigi Alfredo Grieco. 2019. Quakesense, a LoRa-compliant earthquake monitoring open system. In *Proceedings of the International Symposium on Distributed Simulation and Real Time Applications (DS-RT '19)*. IEEE/ACM.

[5] Stefano Buzzi and H Vincent Poor. 2001. Channel estimation and multiuser detection in long-code DS/CDMA systems. *IEEE Journal on Selected Areas in Communications* 19, 8 (2001), 1476–1487.

[6] Zhaoxin Chang, Fusang Zhang, Jie Xiong, Junqi Ma, Beihong Jin, and Daqing Zhang. 2022. Sensor-free Soil Moisture Sensing Using LoRa Signals. In *Proceedings of the ACM on Interactive, Mobile, Wearable and Ubiquitous Technologies (Ubicomp '22)*. ACM.

[7] Lili Chen, Jie Xiong, Xiaojiang Chen, Sunghoon Ivan Lee, Kai Chen, Dianhe Han, Dingyi Fang, Zhanyong Tang, and Zheng Wang. 2019. WideSee: Towards wide-area contactless wireless sensing. In *Proceedings of the 17th Conference on Embedded Networked Sensor Systems (Sensys '19)*. ACM.

[8] Qian Chen and Jiliang Wang. 2021. AlignTrack: Push the Limit of LoRa Collision Decoding. In *Proceedings of the International Conference on Network Protocols (ICNP '21)*. IEEE.

[9] Tonghao Chen, Derek Eager, and Dwight Makaroff. 2019. Efficient image transmission using lora technology in agricultural monitoring iot systems. In *Proceedings of the International Conference on Internet of Things (iThings '19)*. IEEE.

[10] X Ascar Davix and D Judson. 2019. Successive interference cancellation in asynchronous CC-CDMA systems under Rician fading channels. *Telecommunication systems* 72, 1 (2019), 261–271.

[11] Ivo Bizon Franco De Almeida, Luciano Leonel Mendes, Joel JPC Rodrigues, and Mauro AA Da Cruz. 2019. 5G waveforms for IoT applications. *IEEE Communications Surveys & Tutorials* 21, 3 (2019), 2554–2567.

[12] Rashad Eletreby, Diana Zhang, Swarun Kumar, and Osman Yağan. 2017. Empowering low-power wide area networks in urban settings. In *Proceedings of the Conference of the ACM Special Interest Group on Data Communication (SIGCOMM '17)*. ACM.

[13] Lin Fang and Laurence B Milstein. 2000. Successive interference cancellation in multicarrier DS/CDMA. *IEEE Transactions on communications* 48, 9 (2000), 1530–1540.

[14] Branden Ghena, Joshua Adkins, Longfei Shangguan, Kyle Jamieson, Philip Levis, and Prabal Dutta. 2019. Challenge: Unlicensed lpwans are not yet the path to ubiquitous connectivity. In *Proceedings of the International Conference on Mobile Computing and Networking (MobiCom '19)*. ACM.

[15] AK Gnanasekar and V Nagarajan. 2020. Efficient MAI Cancellation Scheme in MC-DS-CDMA Using SIC. *International Journal of Parallel Programming* 48, 1 (2020), 416–430.

[16] Shyamnath Gollakota and Dina Katabi. 2008. Zigzag decoding: Combating hidden terminals in wireless networks. In *Proceedings of the Conference of the ACM Special Interest Group on Data Communication (SIGCOMM '08)*. ACM.

[17] Olga Goussevskaia and Roger Wattenhofer. 2012. Scheduling wireless links with successive interference cancellation. In *Proceedings of the International Conference on Computer Communications and Networks (ICCCN '12)*. IEEE.

[18] Xiuzhen Guo, Longfei Shangguan, Yuan He, Nan Jing, Jiacheng Zhang, Haotian Jiang, and Yunhao Liu. 2022. Saiyan: Design and Implementation of a Low-power Demodulator for LoRa Backscatter Systems. In *Proceedings of the Symposium on Networked Systems Design and Implementation (NSDI '22)*. USENIX.

[19] Xiuzhen Guo, Longfei Shangguan, Yuan He, Jia Zhang, Haotian Jiang, Awais Ahmad Siddiqi, and Yunhao Liu. 2020. Aloba: rethinking ON-OFF keying modulation for ambient LoRa backscatter. In *Proceedings of the Conference on Embedded Networked Sensor Systems (Sensys '20)*. ACM.

[20] Mehrdad Hessar, Ali Najafi, and Shyamnath Gollakota. 2019. NetScatter: Enabling Large-Scale Backscatter Networks. In *Proceedings of the Symposium on Networked Systems Design and Implementation (NSDI '19)*. USENIX.

[21] Steven Hong, Joel Brand, Jung Il Choi, Mayank Jain, Jeff Mehlman, Sachin Katti, and Philip Levis. 2014. Applications of self-interference cancellation in 5G and beyond. *IEEE Communications Magazine* 52, 2 (2014), 114–121.

[22] Ningning Hou and Yuanqing Zheng. 2021. Cloaklora: A covert channel over LoRa phy. In *Proceedings of the International Conference on Network Protocols (ICNP '21)*. IEEE.

[23] Shinnosuke Iino and Makoto Itami. 2021. Performance Evaluation of DS-CDMA IVC Based on Location-Oriented Code Allocation and Performance Improvement Using SIC in Urban Environment. *Journal of Signal Processing* 25, 4 (2021), 133–136.

[24] Jinyan Jiang, Zhenqiang Xu, Fan Dang, and Jiliang Wang. 2021. Long-range ambient LoRa backscatter with parallel decoding. In *Proceedings of the Annual International Conference on Mobile Computing and Networking (Mobicom '21)*. ACM.

[25] Huang-Chen Lee and Kai-Hsiang Ke. 2018. Monitoring of large-area IoT sensors using a LoRa wireless mesh network system: Design and evaluation. *IEEE Transactions on Instrumentation and Measurement* 67, 9 (2018), 2177–2187.

[26] Chenning Li, Xiuzhen Guo, Longfei Shangguan, Zhichao Cao, and Kyle Jamieson. 2020. CurvingLoRa to Boost LoRa Network Capacity via Concurrent Transmission. In *Proceedings of the USENIX Symposium on Networked Systems Design and Implementation (NSDI '22)*. USENIX.

[27] Li Erran Li, Kun Tan, Harish Viswanathan, Ying Xu, and Yang Richard Yang. 2010. Retransmission≠ repeat: simple retransmission permutation can resolve overlapping channel collisions. In *Proceedings of the sixteenth annual international conference on Mobile computing and networking (Mobicom '10)*. ACM.

[28] Konstantin Mikhaylov, Juha Petäjäjärvi, and Janne Janhunen. 2017. On LoRaWAN scalability: Empirical evaluation of susceptibility to inter-network interference. In *Proceedings of the European Conference on Networks and Communications (EuCNC '17)*. IEEE.

[29] Arunesh Mishra, Vivek Shrivastava, Suman Banerjee, and William Arbaugh. 2006. Partially overlapped channels not considered harmful. In *Proceedings of the joint international conference on Measurement and modeling of computer systems (SIGMETRICS '06)*. ACM.

[30] Lufeng Mo, Yuan He, Yunhao Liu, Jizhong Zhao, Shao-Jie Tang, Xiang-Yang Li, and Guojun Dai. 2009. Canopy closure estimates with greenorbs: Sustainable sensing in the forest. In *Proceedings of the 7th ACM Conference on Embedded Networked Sensor Systems (Sensys '09)*. ACM.

[31] Mohsen Mollanoori and Majid Ghaderi. 2013. Uplink scheduling in wireless networks with successive interference cancellation. *IEEE Transactions on Mobile Computing* 13, 5 (2013), 1132–1144.

[32] P. Patel and J. Holtzman. 1994. Analysis of a simple successive interference cancellation scheme in a DS/CDMA system. *IEEE Journal on Selected Areas in Communications* 12, 5 (1994), 796–807.

[33] Yao Peng, Longfei Shangguan, Yue Hu, Yujie Qian, Xianshang Lin, Xiaojiang Chen, Dingyi Fang, and Kyle Jamieson. 2018. PLoRa: A passive long-range data network from ambient LoRa transmissions. In *Proceedings of the conference of the ACM special interest group on data communication (SIGCOMM '18)*. ACM.

[34] Ashutosh Sabharwal, Urbashi Mitra, and Randolph Moses. 2001. MMSE receivers for multirate DS-CDMA systems. *IEEE Transactions on Communications* 49, 12 (2001), 2184–2197.

[35] Vincent Savaux and Patrick Savelli. 2021. Frequency domain preamble-based channel estimation and equalisation in LoRa. *International Journal of Mobile Network Design and Innovation* 10, 2 (2021), 74–81.

[36] Semtech. 2019. *SX1301 LoRa Core Digital Baseband Chip*. https://www.semtech.com/products/wireless-rf/lora-core/sx1301

[37] Semtech. 2019. *SX1302 LoRa Core Digital Baseband Chip*. https://www.semtech.com/products/wireless-rf/lora-core/sx1302

[38] Souvik Sen, Naveen Santhapuri, Romit Roy Choudhury, and Srihari Nelakuditi. 2012. Successive interference cancellation: Carving out MAC layer opportunities. *IEEE Transactions on Mobile Computing* 12, 2 (2012), 346–357.

[39] Muhammad Osama Shahid, Millan Philipose, Krishna Chintalapudi, Suman Banerjee, and Bhuvana Krishnaswamy. 2020. Concurrent interference cancellation: decoding multi-packet collisions in LoRa. In *Proceedings of the Special Interest Group on Data Communication (SIGCOMM '20)*. ACM.

[40] Nicolas Sornin and Ludovic Champion. 2017. Signal concentrator device. US Patent 9,794,095.

[41] Anestis Staikopoulos, Venetis Kanakaris, and George A Papakostas. 2020. Image Transmission via LoRa Networks–A Survey. In *Proceedings of the International Conference on Image, Vision and Computing (ICIVC '20)*. IEEE.

[42] Shuai Tong, Zilin Shen, Yunhao Liu, and Jiliang Wang. 2021. Combating link dynamics for reliable lora connection in urban settings. In *Proceedings of the Annual International Conference on Mobile Computing and Networking (Mobicom '21)*. ACM.

[43] Shuai Tong, Jiliang Wang, and Yunhao Liu. 2020. Combating packet collisions using non-stationary signal scaling in LPWANs. In *Proceedings of the International Conference on Mobile Systems, Applications, and Services (MobiSys '20)*. ACM.

[44] Shuai Tong, Zhenqiang Xu, and Jiliang Wang. 2020. Colora: Enabling multi-packet reception in lora. In *Proceedings of the International Conference on Computer Communications (INFOCOM '20)*. IEEE.

[45] Thiemo Voigt, Martin Bor, Utz Roedig, and Juan Alonso. 2017. Mitigating Inter-network Interference in LoRa Networks. In *Proceedings of the International Conference on Embedded Wireless Systems and Networks (EWSN '17)*. ACM.

[46] Lu Wang, Xiaoke Qi, Ruifeng Huang, Kaishun Wu, and Qian Zhang. 2022. Exploring Partially Overlapping Channels for Low Power Wide Area Networks. *ACM Transactions on Sensor Networks* (2022).

[47] Xiong Wang, Linghe Kong, Liang He, and Guihai Chen. 2019. MLoRa: A multi-packet reception protocol in LoRa networks. In *Proceedings of the International Conference on Network Protocols (ICNP '19)*. IEEE.

[48] Yuting Wang, Xiaolong Zheng, Liang Liu, and Huadong Ma. 2022. PolarTracker: Attitude-aware channel access for floating low power wide area networks. *IEEE/ACM Transactions on Networking* 30, 4 (2022), 1807–1821.

[49] Chinc-Chuan Wei, Jia-Kai Huang, Chia-Chi Chang, and Kuan-Chun Chang. 2020. The Development of LoRa Image Transmission Based on Time Division Multiplexing. In *Proceedings of the International Symposium on Computer, Consumer and Control (IS3C '20)*. IEEE.

[50] Ching-Chuan Wei, Pei-Yi Su, Chia-Chi Chang, and Kuan-Chun Chang. 2021. A study on LoRa Dynamic Image Transmission. In *Proceedings of the International Conference on Knowledge Innovation and Invention (ICKII '21)*. IEEE.

[51] Xianjin Xia, Yuanqing Zheng, and Tao Gu. 2019. FTrack: Parallel Decoding for LoRa Transmissions. In *Proceedings of the Conference on Embedded Networked Sensor Systems (SenSys '19)*. ACM.

[52] Binbin Xie and Jie Xiong. 2020. Combating interference for long range LoRa sensing. In *Proceedings of the Conference on Embedded Networked Sensor Systems (Sensys '20)*. ACM.

[53] Binbin Xie, Yuqing Yin, and Jie Xiong. 2021. Pushing the limits of long range wireless sensing with lora. In *Proceedings of the ACM on Interactive, Mobile, Wearable and Ubiquitous Technologies (Ubicomp '21)*. ACM.

[54] Xing Xu, Ji Luo, and Qian Zhang. 2010. Design of non-orthogonal multi-channel sensor networks. In *Proceedings of the 30th International Conference on Distributed Computing Systems (ICDCS '10)*. IEEE.

[55] Zhenqiang Xu, Pengjin Xie, and Jiliang Wang. 2021. Pyramid: Real-time lora collision decoding with peak tracking. In *Proceedings of the International Conference on Computer Communications (INFOCOM '21)*. IEEE.

[56] Fu Yu, Xiaolong Zheng, Liang Liu, and Huadong Ma. 2022. LoRadar: An efficient LoRa channel occupancy acquirer based on cross-channel scanning. In *Proceedings of the International Conference on Computer Communications (INFOCOM '22)*. IEEE.